Hindawi
Journal of Robotics
Volume 2022, Article ID 6406672, 9 pages
https://doi.org/10.1155/2022/6406672

Research Article

Infrared Fast-Maneuvering Target Tracking Based on Robust Exact Differentiator with Improved Particle Filter

Wanxin Zhang,[1] **Bingrui Huang**,[1] **Sijie Meng**,[2] **and Jihong Zhu**[3]

[1]*School of Automation, Beijing University of Posts and Telecommunications, Beijing, China*
[2]*School of Economics and Management of Beijing University of Posts and Telecommunications, Beijing, China*
[3]*Department of Precision Instrument, Tsinghua University, Beijing, China*

Correspondence should be addressed to Wanxin Zhang; zhangwanxin@bupt.edu.cn

Received 22 August 2022; Accepted 13 September 2022; Published 21 October 2022

Academic Editor: Shuofei Yang

This paper deals with the problem of nonlinear uncertainties when tracking an infrared dim small target with fast maneuvers. The particle filter (PF)-based methods are mostly considered. The existing improvement methods for the PF can handle the infrared dim small target with the conventional maneuver, the motion state of which changes slowly and in most cases is assumed to be linear. However, when fast maneuvers appear on the target, the PF-based method will soon suffer from particle degeneracy, or even loss of the target. In this paper, a robust exact differentiator (RED)-based particle generating method is proposed to improve the PF. New birth particles are produced by the proposed method, which can keep up with the fast maneuvers, and ensure the particle diversity of the PF, so as to avoid the particle degeneracy and depletion, meanwhile the number of particles required can be decreased. Numerical simulations are conducted, showing that the proposed algorithm has more advantages than the state-of-the-art method.

1. Introduction

The target tracking technology estimates and predicts the motion state of the target by establishing a motion model [1, 2] and integrating filtering methods [3], based on the data information obtained from radar, infrared imaging system, or other sensors [4–6]. Traditional target tracking technology adopts the detect-before-track (DBT) method, which directly uses the original observation date obtained from the sensors with low thresholds and mines the data information. Through the integration of observations over time, the signal-to-noise ratio can be improved, so as to achieve the tracking of the target. The DBT method works well under high signal-to-noise ratio, however, cannot handle the target well under low signal-to-noise ratio. The track-before-detect (TBD) method is then introduced by scholars, which can handle weak target with good effects through noncoherent integration [7]. The TBD method searches for the target trajectory from multiple frames of data and accumulates the energy along the trajectory. The key problem of the method is how to obtain the prior information about the target.

Fast maneuvering targets, such as vehicles, aircrafts, and missiles, are able to change the motion states with quick speed, or big acceleration in a short time [8], so as to realize the maneuvering motivation, which will bring nonlinear uncertainties to the information about the target [9]. Due to the nonlinear uncertainty of the target model [10, 11], the traditional Kalman filter (KF) [12] is not applicable. Besides, an infrared dim small target in a complex background will also bring difficulties to filters. Infrared image is obtained by making use of the intensity of infrared light of the object. Different objects or different parts of the same object in most cases have different thermal radiation characteristics, such as temperature and emissivity. Through the infrared imaging system, the differences are converted into electrical signals, and then the electrical signals are converted into visible light images. Infrared image is generally dim, with low contrast resolution between the target image and background, and

the noise, meanwhile is large, which affects the subsequent processing of the image.

In recent years, the particle filter (PF)-based methods have been used to detect and track targets, [13–16] and have performed good results on tracking dim small targets [16, 17]. Different from the KF, the PF can get rid of the limitations of linear and Gaussian assumptions [18]. However, the PF has two major problems. One is the large number of samples required to approximate the posteriori probability density. When the background is complex, the sample size should be huge, which consequently increases the algorithm complexity. The other is the sample depletion. The resampling process abandons particles with low weights, which will cause the loss of diversity and effectiveness in particles after iterations for times, resulting in particle degeneracy and sample depletion. Studies [19–21] show that these two problems of the PF are particular serious on tracking non-Gaussian targets with strong nonlinearities.

Aiming at solving the two problems of the PF, this paper proposed a new target tracking method, with which the PF can be ensured to keep up with the change of the target motion when the target is highly maneuvered, and meanwhile the target motion trajectory can be estimated accurately.

The rest of this paper is organized as follows: Section 2 reviews related works on the PF method and the KF method. Section 3 develops the robust exact differentiator (RED)-based particle generating method and improved PF algorithm. Section 4 discusses experimental results and, finally, Section 5 concludes the paper.

2. Related Work

The tracking ability of the filter is usually determined by the reasonable mathematical model of the target motion. However, in the real situation, the motion law of the target will be affected by many factors [22, 23], which causes a mismatch between the target motion and the filtering model. The state of the target, consequently, cannot be estimated accurately. Denote the state vector of the target at time k as $\{\mathbf{x}_k, k \in N\}$, which consists of the position, the speed, and the acceleration of the target, with size of n_x. Denote the observation vector of the target at time k as $\{\mathbf{z}_k, k \in N\}$ with size of n_z. Then, the state model and observation model can be described as follows:

$$\begin{aligned} \mathbf{x}_k &= \mathbf{f}_k(\mathbf{x}_{k-1}, \mathbf{u}_{k-1}), \\ \mathbf{z}_k &= \mathbf{g}_k(\mathbf{x}_k, \mathbf{v}_k), \end{aligned} \tag{1}$$

where $\mathbf{f}_k$ and $\mathbf{g}_k$ are the nonlinear functions of the state vector, representing the state transition function and the observation function, respectively, $\mathbf{u}_{k-1}$ is the process noise vector of the discrete system, and $\mathbf{v}_k$ is the observation noise vector.

2.1. PF. The PF is a sequential Monte Carlo method, with the idea which makes use of the weighted random samples and the estimations based on these samples to achieve the posterior probability density $p(\mathbf{x}_k|\mathbf{z}_{1:k})$. $\mathbf{z}_k$ corresponds to the infrared image measurements obtained from infrared sensors at frame k.

Denote the random sample set of the posterior probability density $p(\mathbf{x}_k|\mathbf{z}_{1:k})$ as $\{\mathbf{x}_k^i, w_k^i\}_{i=1}^{N_k}$, where $\mathbf{x}_k^i$ is the i th particle at frame k, w_k^i is the weight of the particle $\mathbf{x}_k^i$, and N_k is the number of particles. Normalization processing is usually made that $\sum_i w_k^i = 1$. The posterior probability density is given as follows:

$$p(\mathbf{x}_k|\mathbf{z}_{1:k}) \approx \sum_{i=1}^{N_k} w_k^i \delta\left(\mathbf{x}_k - \mathbf{x}_k^i\right). \tag{2}$$

w_k^i is updated by the following recursive equations [24]:

$$w_{k|k-1}^i \propto w_{k-1}^i \frac{p\left(\mathbf{x}_k^i|\mathbf{x}_{k-1}^i\right)}{q\left(\mathbf{x}_k^i|\mathbf{x}_{k-1}^i, \mathbf{z}_k\right)}, \tag{3}$$

$$w_k^i \propto w_{k|k-1}^i p\left(\mathbf{z}_k|\mathbf{x}_k^i\right), \tag{4}$$

where $q(\mathbf{x}_k^i|\mathbf{x}_{k-1}^i, \mathbf{z}_k)$ is the importance density, of which three forms are commonly used [25]:

(i) the prior probability $q(\mathbf{x}_k^i|\mathbf{x}_{k-1}^i, \mathbf{z}_k) = p(\mathbf{x}_k^i|\mathbf{x}_{k-1}^i)$;

(ii) the likelihood $q(\mathbf{x}_k^i|\mathbf{x}_{k-1}^i, \mathbf{z}_k) = p(\mathbf{z}_k|\mathbf{x}_k^i)$; and

(iii) the optimal by minimizing the weight variance $q(\mathbf{x}_k^i|\mathbf{x}_{k-1}^i, \mathbf{z}_k) = p(\mathbf{z}_k|\mathbf{x}_k^i)p(\mathbf{x}_k^i|\mathbf{x}_{k-1}^i)$.

Denote the weighted particle set with joint state vector as $\{\mathbf{x}_k^i, e_k^i, w\}_{i=1}^{N_k}$, where $e_k^i = 1$ indicates that the target exists, and $e_k^i = 0$ indicates that the target is absent. Resample from the previous particle set and newly weighted particle set. Finally, the position of the target can be estimated by the following equation:

$$\mathbf{x}_k = \frac{\sum_{i=1}^{N_k} \mathbf{x}_k^i \cdot e_k^i}{\sum_{i=1}^{N_k} e_k^i}. \tag{5}$$

2.2. KF. The KF always makes an assumption that the system can be regarded to be linear and Gaussian, so the model in (1) needs to be simplified as follows:

$$\begin{aligned} \mathbf{x}_k &= \mathbf{F}_{k-1}\mathbf{x}_{k-1} + \mathbf{u}_{k-1}, \\ \mathbf{z}_k &= \mathbf{G}_k\mathbf{x}_k + \mathbf{v}_k, \end{aligned} \tag{6}$$

where $\mathbf{F}$ is the linearized form of $\mathbf{f}$ in (1), representing the state transition matrix, and $\mathbf{G}$ is the linearized form of $\mathbf{g}$ in (1), representing the observation matrix.

$\mathbf{u}$ and $\mathbf{v}$ are assumed to be mutually independent, with a zero mean and covariance matrices $\mathbf{Q}$ and $\mathbf{R}$, respectively,

$$\begin{aligned} \mathbf{u}_k &\sim \mathcal{N}(0, \mathbf{Q}_k), \\ \mathbf{v}_k &\sim \mathcal{N}(0, \mathbf{R}_k). \end{aligned} \tag{7}$$

The KF searches for the optimal solution by minimizing the mean square error,

$$\widehat{\mathbf{x}}_{\text{opt}} = \text{argmin}_{\widehat{\mathbf{x}}} E\left\{(\widehat{\mathbf{x}} - \mathbf{x})^T (\widehat{\mathbf{x}} - \mathbf{x})\right\}. \tag{8}$$

Denote the estimation of $\mathbf{x}$ at frame n given the observations of frame k that $k \le m$ as $\hat{\mathbf{x}}_{n|m}$. Denote the error covariance matrix as $\mathbf{P}_{n|m}$ with $\mathbf{P}_{n|m} = \mathrm{cov}(\mathbf{x}_n - \hat{\mathbf{x}}_{n|m})$. The predictions of $\hat{\mathbf{x}}$ and $\mathbf{P}$ are given as follows:

$$\begin{aligned} \hat{\mathbf{x}}_{k+1|k} &= \mathbf{F}_k \hat{\mathbf{x}}_{k|k}, \\ \mathbf{P}_{k+1|k} &= \mathbf{F}_k \mathbf{P}_{k|k} \mathbf{F}_k^T + \mathbf{Q}_k. \end{aligned} \tag{9}$$

Then

$$\begin{aligned} \hat{\mathbf{x}}_{k+1|k+1} &= \hat{\mathbf{x}}_{k+1|k} + \mathbf{K}_{k+1}\left(\mathbf{z}_{k+1} - \mathbf{G}_k \hat{\mathbf{x}}_{k+1|k}\right), \\ \mathbf{P}_{k+1|k+1} &= \left(\mathbf{I} - \mathbf{K}_{k+1}\mathbf{G}_{k+1}\right)\mathbf{P}_{k+1|k}, \end{aligned} \tag{10}$$

where the gain matrix $\mathbf{K}$ is given by

$$\mathbf{K}_{k+1} = \mathbf{P}_{k+1|k}\mathbf{G}_k^T\left(\mathbf{G}_k \mathbf{P}_{k+1|k}\mathbf{G}_k^T + \mathbf{R}_k\right)^{-1}. \tag{11}$$

3. Approach

To handle the maneuvering target, the KF usually makes the assumption of constant acceleration. The state vector $\mathbf{x}_k$ is defined as follows:

$$\mathbf{x}_k = \left[x_k, \dot{x}_k, \ddot{x}_k, y_k, \dot{y}_k, \ddot{y}_k\right]^T, \tag{12}$$

where x_k is the x position of the target in the infrared image at frame k, y_k is the y position of the target in the infrared image at frame k, $\dot{x}_k$ and $\dot{y}_k$ are speeds along x-axis and y-axis, and $\ddot{x}_k$ and $\ddot{y}_k$ are accelerations along x-axis and y-axis.

Based on the assumption of constant acceleration that the acceleration of the target is constant in small time interval [26, 27], the state and observation equations can be obtained as follows:

$$\begin{aligned} \mathbf{x}_k &= \begin{pmatrix} 1 & \Delta t & \Delta t^2/2 & & & \\ 0 & 1 & \Delta t & & 0 & \\ 0 & 0 & 1 & & & \\ & & & 1 & \Delta t & \Delta t^2/2 \\ & 0 & & 0 & 1 & \Delta t \\ & & & 0 & 0 & 1 \end{pmatrix} \mathbf{x}_{k-1} + \mathbf{u}_{k-1}, \\ \mathbf{z}_k &= \begin{bmatrix} 0 & 0 & 1 & 0 & 0 & 0 \\ 0 & 0 & 0 & 0 & 0 & 1 \end{bmatrix} \mathbf{x}_k + \mathbf{v}_k, \end{aligned} \tag{13}$$

where Δt is the time interval between adjacent frames.

Considering the situations that the target maneuvers at a fast-varying speed, the assumption of constant acceleration is no longer suitable. This paper uses the robust exact differentiation (RED), proposed by Levant, to deal with the practical real-time differentiation problem and obtain the real-time acceleration of the target [28]. We use x_0 to represent the estimation of x-position of the target in the image, x_1 is the estimation of speed along x-axis, and x_2 is the estimation of acceleration along x-axis. The same goes for y. According to the RED based on the supertwisting algorithm [29], the tracking observation model of $\{x_1, x_2, x_3, y_1, y_2, y_3\}$ is given as follows:

$$\begin{aligned} \dot{x}_0 &= -\lambda_2 L_x^{1/3}\left|x_0 - x(t)\right|^{2/3}\mathrm{sign}\left(x_0 - x(t)\right) + x_1, \\ \dot{x}_1 &= -\lambda_1 L_x^{2/3}\left|x_0 - x(t)\right|^{1/3}\mathrm{sign}\left(x_0 - x(t)\right) + x_2, \\ \dot{x}_2 &= -\lambda_0 L_x \mathrm{sign}\left(x_0 - x(t)\right), \\ \dot{y}_0 &= -\lambda_2 L_y^{1/3}\left|y_0 - y(t)\right|^{2/3}\mathrm{sign}\left(y_0 - y(t)\right) + y_1, \\ \dot{y}_1 &= -\lambda_1 L_y^{2/3}\left|y_0 - y(t)\right|^{1/3}\mathrm{sign}\left(y_0 - y(t)\right) + y_2, \\ \dot{y}_2 &= -\lambda_0 L_y \mathrm{sign}\left(y_0 - y(t)\right), \end{aligned} \tag{14}$$

where $x(t), y(t)$ are measurable locally bounded functions, having derivatives with Lipschitz constants $L_x > 0$, and $L_y > 0$, $\lambda_0, \lambda_1, \lambda_2 > 0$ are the gain parameters.

Apart from the persisting particles, we generate new birth particles according to the estimations obtained from Algorithm 1, with the importance density of $\beta(\mathbf{x}|\hat{\mathbf{x}})$. The weights of the new birth particles are given by [30].

$$w_k^i = \frac{b_k\left(\mathbf{x}_k^i\right)}{\beta_k\left(\mathbf{x}_k^i|\hat{\mathbf{x}}_k\right)}\frac{1}{\hat{N}_k}, \quad i = N_k + 1, \ldots, N_k + \hat{N}_k, \tag{15}$$

where $\hat{N}_k$ is the number of new birth particles and $b_k(\mathbf{x}_k^i)$ is given by the uniform distribution over the state space around the target predictions of Algorithm 1.

The flow chart of the proposed algorithm as a whole is shown in Figure 1. At the initial stage, the tracking target is specified manually. Then, the features of the target are calculated. At the searching stage, the particles are uniformly assigned. Then, the weights of the particles are updated according to the results of similarity calculation. Based on the updated weights, the efficient number of particles is calculated.

$$N_{\mathrm{eff}}^k = \frac{1}{\sum_{i=1}^{N}\left(w_k^i\right)^2}. \tag{16}$$

The efficient number is the indicator to determine whether to generate new particles. Particle resampling process is then conducted. By repeating the abovementioned processes for several times, the most likely place for the target will be calculated. Algorithm 2 describes the iteration of the improved PF.

4. Experiments

The experiments adopt the dataset download from https://www.dx.doi.org/10.11922/sciencedb.902 [31]. The dataset contains image sequences for tracking low altitude flying dim small targets. Fast maneuvers are also included in some of the image sequences.

Image preprocessing is firstly made. To reduce the noise, the images are improved by enhancing the information required and weakening the information unwanted. The original small range of gray value is broadened. Then, image segmentation is carried out to make the target separated from the background.

We compare the proposed method with the basic PF and KF-PF. For the convenience of intuitive understanding, we name our method as RED-KF-PF. The three methods give the same parameter settings for KF and PF in the

Inputs: $\mathbf{z}_k, \Delta T$
Outputs: $\hat{\mathbf{x}}_k, \hat{\mathbf{x}}_{k+1}$
(1) Initialization: declare and initialize variables $x_0, x_1, x_2, y_0, y_1, y_2, \hat{\mathbf{x}}_0, \mathbf{P}_0$.
(2) Declare differentiator parameters and filter parameters $\lambda_0 = 1.1$, $\lambda_1 = 2.12$, $\lambda_2 = 2$, η, and ε, Lipschitz constants L_x, L_y, and the covariance matrices $\mathbf{Q}$ and $\mathbf{R}$.
(3) while not convergent do
(4) if $\|\mathbf{z}_k - \hat{\mathbf{x}}_k\|_\infty < \eta$ then {Case 1 KF}
(5) According to (10)-(14), update $\hat{\mathbf{x}}_{k+1|k}$, $\mathbf{P}_{k+1|k}$, $\hat{\mathbf{x}}_{k+1|k+1}$, $\mathbf{P}_{k+1|k+1}$, and $\mathbf{K}_{k+1}$ in sequence based on the constant acceleration model in (6)
(6) else {Case 2 RED}
(7) $\dot{x}_0 = -\lambda_2 L_x^{1/3} |x_0 - z_x(k)|^{2/3} \operatorname{sign}(x_0 - z_x(k)) + x_1$
(8) $\dot{x}_1 = -\lambda_1 L_x^{2/3} |x_0 - z_x(k)|^{1/3} \operatorname{sign}(x_0 - z_x(k)) + x_2$
(9) $\dot{x}_2 = -\lambda_0 L_x \operatorname{sign}(x_0 - z_x(k))$
(10) $\dot{y}_0 = -\lambda_2 L_y^{1/3} |y_0 - z_y(k)|^{2/3} \operatorname{sign}(y_0 - z_y(k)) + y_1$
(11) $\dot{y}_1 = -\lambda_1 L_y^{2/3} |y_0 - z_y(k)|^{1/3} \operatorname{sign}(y_0 - z_y(k)) + y_2$
(12) $\dot{y}_2 = -\lambda_0 L_y \operatorname{sign}(y_0 - z_y(k))$
(13) Integrate variables $\dot{x}_0$, $\dot{x}_1$, $\dot{x}_2$, $\dot{y}_0$, $\dot{y}_1$, and $\dot{y}_2$ over ΔT to obtain $x_0, x_1, x_2, y_0, y_1, y_2$
(14) end if
(15) Check the convergence conditions: $\|\hat{\mathbf{x}}_k - \mathbf{z}_k\|_\infty < \varepsilon$
(16) end while

Algorithm 1: Calculating the center of newly generated particles by the proposed method.

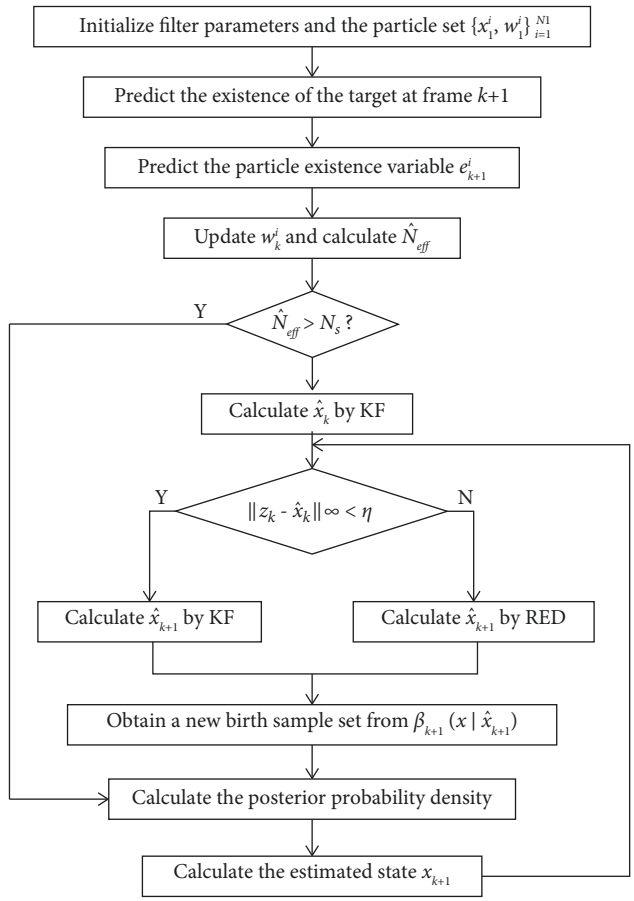

Figure 1: Flow chart of the proposed algorithm.

Inputs: $\mathbf{z}_k$, $\widehat{\mathbf{x}}_{k+1}$
Outputs: $\mathbf{x}_{k+1}$
(1) Initialization: declare the particle representation $\{\mathbf{x}_{1,e}^i, 1, w_{1,e}^i\}_{i=1}^{N_1^e}$, $\{\mathbf{x}_{1,a}^i, 0, w_{1,a}^i\}_{i=1}^{N_1^a}$.
(2) $\{\mathbf{x}_k^i, w_k^i\}_{i=1}^{N_k} = \{\mathbf{x}_{k,e}^i, w_{k,e}^i\}_{i=1}^{N_k^e} \cup \{\mathbf{x}_{k,a}^i, w_{k,a}^i\}_{i=1}^{N_k^a}$
(3) for $k = 1{:}n$ do
(4) $\mathbf{x}_{k+1|k}^i \sim \rho_{k+1}(\mathbf{x}|\mathbf{x}_k^i, \mathbf{z}_{k+1}) \quad i = 1, \ldots, N_k$
(5) $\mathbf{x}_{k+1|k}^i \sim \beta_{k+1}(\mathbf{x}|\widehat{\mathbf{x}}_{k+1}) \quad i = N_k + 1, \ldots, N_k + \widehat{N}_k$
(6) end for
(7) Compute w_k^i, $i = 1, \ldots, N_k$ using (3) and (4).
(8) Compute w_k^i, $i = N_k + 1, \ldots, N_k + \widehat{N}_k$ using (15).
(9) Compute $p = N_k^e/N_k$, $\widehat{p} = \widehat{N}_k^e/\widehat{N}_k$.
(10) Calculate the number of persistent particles in the next step $\widetilde{N}_{k+1} = \lceil N_{k+1}\underline{p}/p + \widehat{p} \rceil$.
(11) Resample $\widetilde{N}_{k+1}$ times from $\{\mathbf{x}_k^i, w_k^i\}_{i=1}^{N_k}$, $\widetilde{N}_{k+1} - \widetilde{N}_{k+1}$ times from $\{\mathbf{x}_k^i, w_k^i\}_{i=N_k+1}^{N_k+N_k}$.
(12) Normalize the weights of the N_{K+1} particles.
(13) Compute $\mathbf{x}_{k+1}$ using (5).

Algorithm 2: The improved PF for the fast-maneuvering target.

Table 1: Comparison of RMSE.

Particle		PF	KF-PF	RED-KF-PF
$N = 100$	x	0.3454	0.1666	0.1437
	y	0.1487	0.0719	0.0530
$N = 500$	x	0.2562	0.1236	0.0971
	y	0.0885	0.0427	0.0359
$N = 1000$	x	0.1014	0.0849	0.0661
	y	0.0373	0.0231	0.0124

Table 2: Comparison of running time.

Particle	PF	KF-PF	RED-KF-PF
$N = 100$	6.4831s	12.5712s	12.4358s
$N = 500$	25.0614s	48.5951s	45.9103s
$N = 1000$	50.5887s	95.1003s	94.1379s

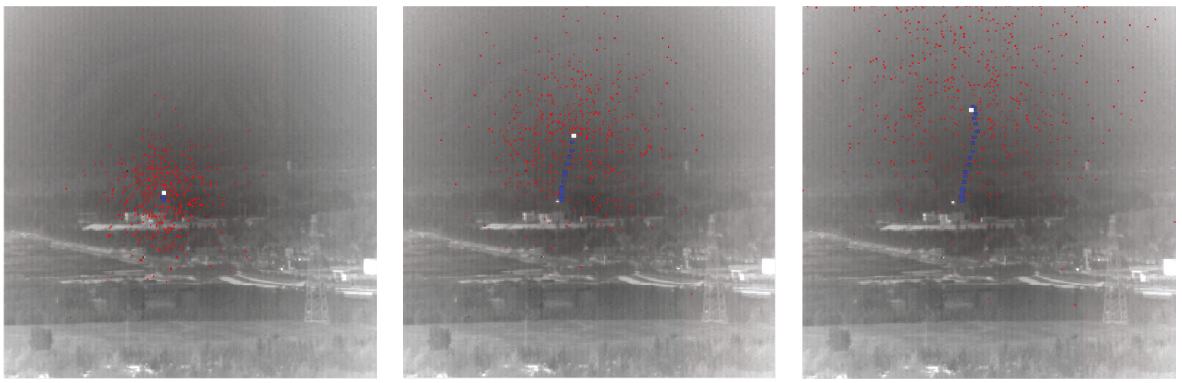

(a) (b) (c)

Figure 2: Continued.

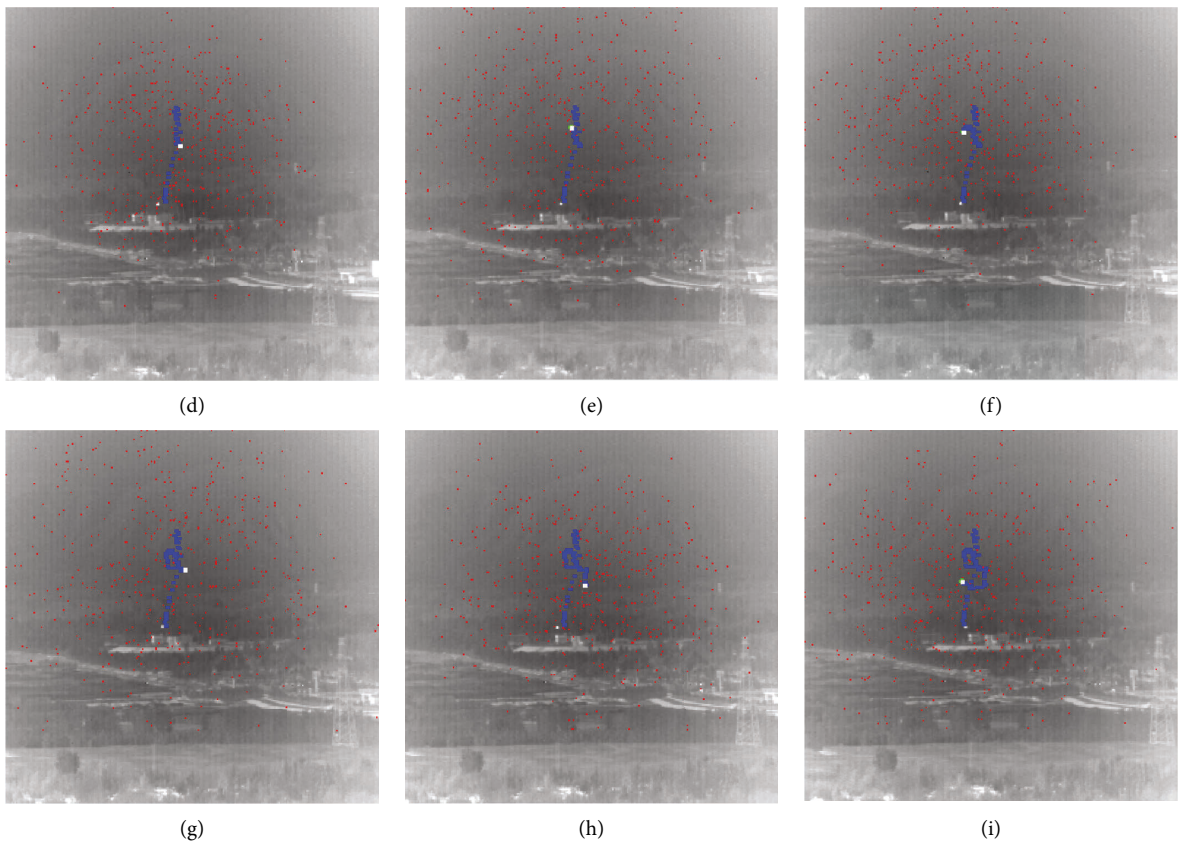

Figure 2: Tracking results of the fast-maneuvering target. The white dot is the target. The blue dot is the estimation of the trajectory. The red dots are particles. (a) The 400th frame. (b) The 410th frame. (c) The 420th frame. (d) The 430th frame. (e) The 440th frame. (f) The 450th frame. (g) The 460th frame. (h) The 470th frame. (i) The 480th frame.

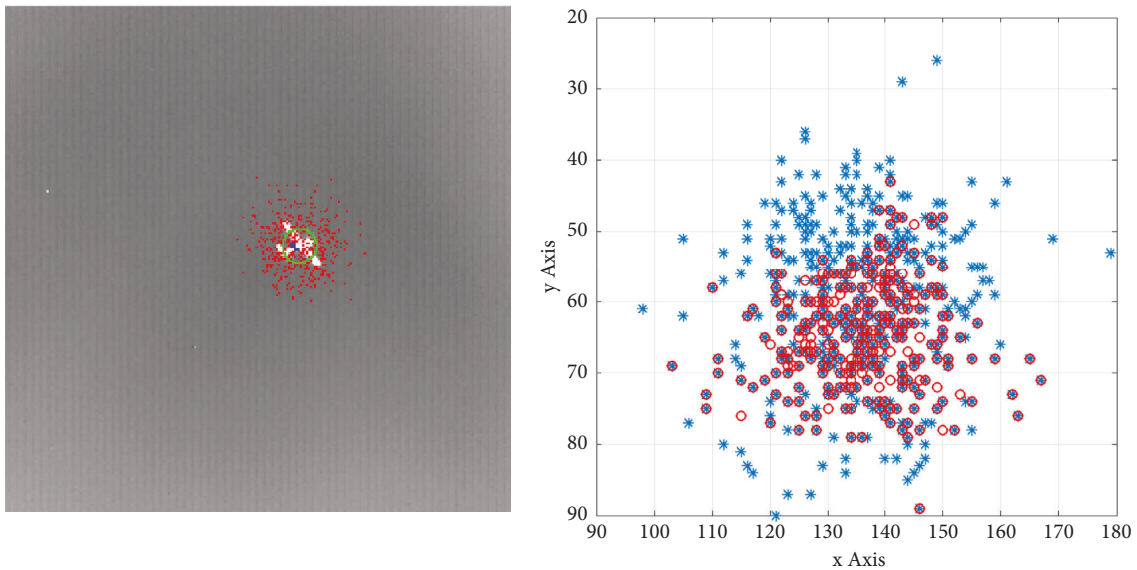

Figure 3: Infrared target characteristics detection. (a) Close target detection. (b) Particle distributions before and after resampling.

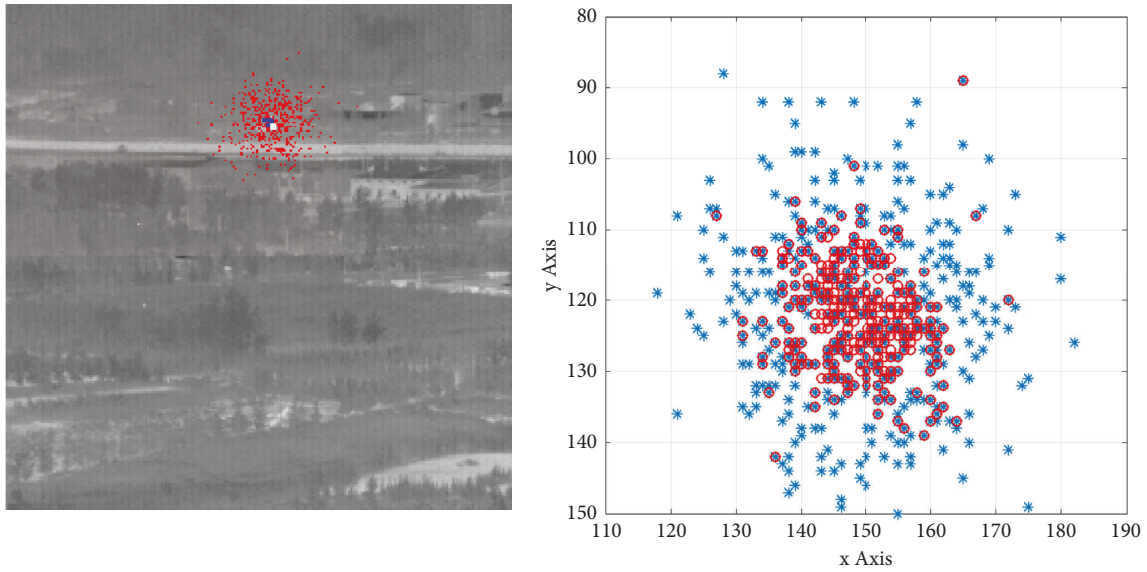

(a) (b)

Figure 4: Dim-small object detection. (a) Distant target detection. (b) Particle distributions before and after resampling.

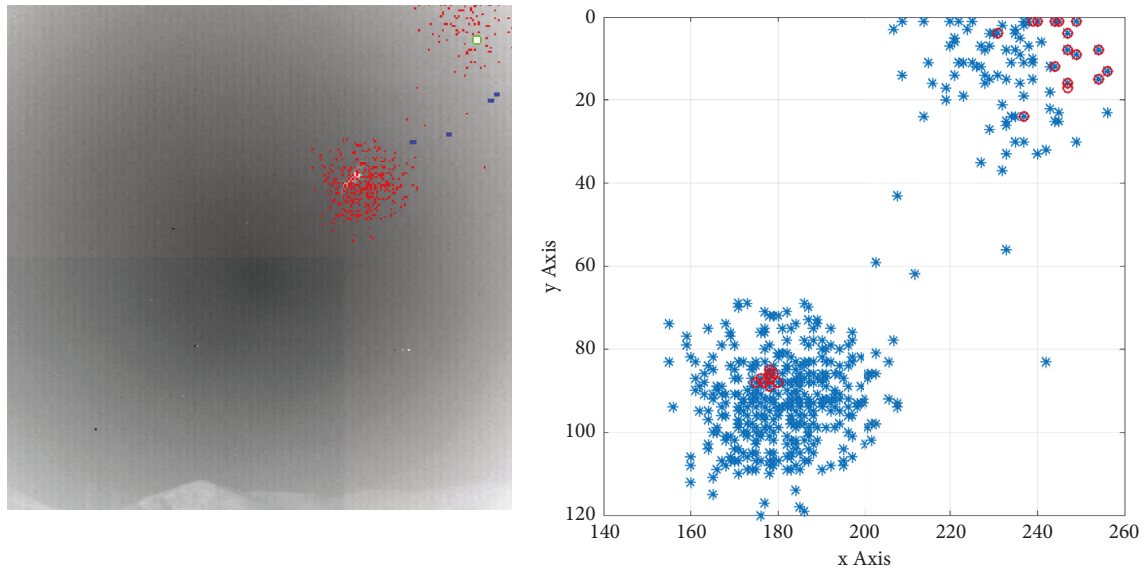

(a) (b)

Figure 5: Fast-maneuvering dim-small target tracking. (a) Fast-maneuvering target detection. (b) Particle distributions before and after resampling.

initialization step so as to guarantee the fairness. The comparison results of RMSE are listed in Table 1. The RMSE is the square root of the mean square error, which is given as follows:

$$\mathrm{RMSE}_x = \sqrt{\frac{1}{N_k}\sum_{i=1}^{N_k}\left(x_k^i - \widehat{x}_k\right)^2}. \tag{17}$$

The comparison results of running time are listed in Table 2. According to Tables 1 and 2, higher accuracy with less particles and less time is achieved by the proposed method.

By choosing the dataset with fast-maneuvering test, Figure 2 demonstrates the tracking process with the proposed algorithm. By choosing the close-range test and the distant-range test, Figures 3 and 4 demonstrate the detection

results and particle distributions. The target takes slow motions, so the particle distributions did not show apparent characteristics of the proposed idea. As in Figure 5, in which a quick maneuver is taken by the target, the particles with great importance mainly come from the RED-based particle generating method. If not, the green dot in Figure 5(a) calculated from the persistent particles would influence the tracking result heavily.

5. Conclusion

To improve the distribution of the particles, the KF with the constant acceleration model is considered to generate particles around the estimation center. In the cases the KF is not capable to track the motions of the target, the RED is constructed to update the estimation center. The generated particles not only improve the diversity of particles but also make the resampled particles much closer to the real target state, so that the PF can approximate the posterior probability density better. Method for modification of the Lipschitz constants L_x and L_y in real time is considered for future work.

Data Availability

All data used during this study are included in this published article [31], and its supplementary information files can be downloaded from https://www.dx.doi.org/10.11922/sciencedb.902.

Conflicts of Interest

The authors declare that they have no conflicts of interest.

Acknowledgments

The authors would like to thank the anonymous reviews for their helpful suggestions to improve the quality of the paper. This work was supported by the Fundamental Research Funds for the Central Universities of China under Grant 2022RC24.

Supplementary Materials

The dataset contains image sequences for tracking low altitude flying dim small targets. The supplementary material file, including 100 frames, provides a group of data for one fixed-wing UAV target with fast maneuvers under complex field background. The dataset can serve research studies on infrared fast-maneuvering target tracking. (*Supplementary Materials*)

References

[1] S. Yang and Y. Li, "Motion generators of quadric surfaces," *Mechanism and Machine Theory*, vol. 140, pp. 446–456, 2019.

[2] S. Yang and Y. Li, "Kinematic analysis of deployable parallel mechanisms," *Proceedings of the Institution of Mechanical Engineers—Part C: Journal of Mechanical Engineering Science*, vol. 234, no. 1, pp. 263–272, 2020.

[3] A. Altan and R. Hacıoğlu, "Model predictive control of three-axis gimbal system mounted on uav for real-time target tracking under external disturbances," *Mechanical Systems and Signal Processing*, vol. 138, Article ID 106548, 2020.

[4] Z. Zhang, C. Huang, D. Ding, S. Tang, B. Han, and H. Huang, "Hummingbirds optimization algorithm-based particle filter for maneuvering target tracking," *Nonlinear Dynamics*, vol. 97, no. 2, pp. 1227–1243, 2019.

[5] Y. Zhu, B. Yi, and T. Guo, "A simple outdoor environment obstacle detection method based on information fusion of depth and infrared," *Journal of Robotics*, vol. 2016, pp. 1–10, 2016.

[6] C. Lersteau, A. Rossi, and M. Sevaux, "Robust scheduling of wireless sensor networks for target tracking under uncertainty," *European Journal of Operational Research*, vol. 252, no. 2, pp. 407–417, 2016.

[7] W. Yi, Z. Fang, W. Li, R. Hoseinnezhad, and L. Kong, "Multi-frame track-before-detect algorithm for maneuvering target tracking," *IEEE Transactions on Vehicular Technology*, vol. 69, no. 4, pp. 4104–4118, 2020.

[8] W. Zhang, M. Xia, and J. Zhu, "Lpv modeling and identification of unsteady aerodynamics for fast maneuvering aircrafts," *IEEE Access*, vol. 7, pp. 92436–92443, 2019.

[9] W. Zhang and J. Zhu, "Online identification of aerodynamics with fast time-varying features using kalman filter," *IET Control Theory & Applications*, vol. 15, no. 2, pp. 272–280, 2021.

[10] M. Tahk and J. L. Speyer, "Target tracking problems subject to kinematic constraints," *IEEE Transactions on Automatic Control*, vol. 35, no. 3, pp. 324–326, 1990.

[11] X. R. Li and V. P. Jilkov, "Survey of maneuvering target tracking. part i. dynamic models," *IEEE Transactions on Aerospace and Electronic Systems*, vol. 39, no. 4, pp. 1333–1364, 2004.

[12] K. György, A. Kelemen, and L. Dávid, "Unscented Kalman filters and particle filter methods for nonlinear state estimation," *Procedia Technology*, vol. 12, pp. 65–74, 2014.

[13] Y. Cheng and T. Singh, "Efficient particle filtering for road-constrained target tracking," *IEEE Transactions on Aerospace and Electronic Systems*, vol. 43, no. 4, pp. 1454–1469, 2007.

[14] J. Lim, "Particle filtering for nonlinear dynamic state systems with unknown noise statistics," *Nonlinear Dynamics*, vol. 78, no. 2, pp. 1369–1388, 2014.

[15] L. C. Chang, S. Pare, M. S. Meena et al., "An intelligent automatic human detection and tracking system based on weighted resampling particle filtering," *Big Data and Cognitive Computing*, vol. 4, no. 4, p. 27, 2020.

[16] S. S. Moghaddasi and N. Faraji, "A hybrid algorithm based on particle filter and genetic algorithm for target tracking," *Expert Systems with Applications*, vol. 147, Article ID 113188, 2020.

[17] D. Pang, T. Shan, W. Li, P. Ma, S. Liu, and R. Tao, "Infrared dim and small target detection based on greedy bilateral factorization in image sequences," *Ieee Journal of Selected Topics in Applied Earth Observations and Remote Sensing*, vol. 13, no. 99, pp. 3394–3408, 2020.

[18] X. Lin, T. Kirubarajan, Y. Bar-Shalom, and S. Maskell, "Comparison of ekf, pseudomeasurement and particle filters for a bearing-only target tracking problem," in *Signal and Data Processing of Small Targets*McMaster University, Malvern, England, 2002.

[19] R. Guo, Z. Qin, X. Li, and J. Chen, "Interacting multiple model particle-type filtering approaches to ground target tracking," *Journal of Computers*, vol. 3, no. 7, 2008.

[20] I. Aranda and G. Perez-Zuniga, "Highly maneuverable target tracking under glint noise via uniform robust exact filtering differentiator with intra pulse median filter," *IEEE Transactions on Aerospace and Electronic Systems*, vol. 58, no. 3, pp. 2541–2559, 2022.

[21] Y. Yu and Q. Cheng, "Particle filters for maneuvering target tracking problem," *Signal Processing*, vol. 86, no. 1, pp. 195–203, 2006.

[22] S. Yang and Y. Li, "Different kinds of 3T2R serial kinematic chains and their applications in synthesis of parallel mechanisms," *Mechanism and Machine Theory*, vol. 144, Article ID 103637, 2020.

[23] S. Yang and Y. Li, "Classification and analysis of constraint singularities for parallel mechanisms using differential manifolds," *Applied Mathematical Modelling*, vol. 77, pp. 469–477, 2020.

[24] Z. Chen, "Bayesian filtering: from kalman filters to particle filters, and beyond," *Statistics: A Journal of Theoretical and Applied Statistics*, vol. 182, no. 1, 2003.

[25] R. L. Streit and T. L. Corwin, *Bayesian Multiple Target Tracking*, Artech House, Inc, Norwood, MA, USA, 1999.

[26] J. Liu and G. Guo, "Pseudolinear Kalman filters for target tracking using hybrid measurements," *Signal Processing*, vol. 188, 2021.

[27] S. Yang, J. S. Dai, Y. Jin, and R. Fu, "Finite displacement screw-based group analysis of 3PRS parallel mechanisms," *Mechanism and Machine Theory*, vol. 171, Article ID 104727, 2022.

[28] H. Ma, Y. Li, and Z. Xiong, "Discrete-time sliding-mode control with enhanced power reaching law," *IEEE Transactions on Industrial Electronics*, vol. 66, no. 6, pp. 4629–4638, 2019.

[29] A. Levant, "Robust exact differentiation via sliding mode technique," *Automatica*, vol. 34, no. 3, pp. 379–384, 1998.

[30] S. Wong, B. T. Vo, and F. Papi, "Bernoulli forward-backward smoothing for track-before-detect," *IEEE Signal Processing Letters*, vol. 21, no. 6, pp. 727–731, 2014.

[31] B. Hui, Z. Song, H. Fan et al., "A dataset for infrared detection and tracking of dim-small aircraft targets under ground/air background[DS/OL]," *Science Data Bank*, 2019.